



HAL
open science

RTS Noise Detection and Voltage Effect on RTS in HgCdTe Focal-Plane Arrays

Maxence Guénin, Sophie Derelle, Marcel Caes, Laurent Rubaldo, Isabelle Ribet-Mohamed

► **To cite this version:**

Maxence Guénin, Sophie Derelle, Marcel Caes, Laurent Rubaldo, Isabelle Ribet-Mohamed. RTS Noise Detection and Voltage Effect on RTS in HgCdTe Focal-Plane Arrays. *Journal of Electronic Materials*, 2020, 49 (11), pp.6963-6970. 10.1007/s11664-020-08271-y . hal-02998334

HAL Id: hal-02998334

<https://hal.science/hal-02998334>

Submitted on 10 Nov 2020

HAL is a multi-disciplinary open access archive for the deposit and dissemination of scientific research documents, whether they are published or not. The documents may come from teaching and research institutions in France or abroad, or from public or private research centers.

L'archive ouverte pluridisciplinaire **HAL**, est destinée au dépôt et à la diffusion de documents scientifiques de niveau recherche, publiés ou non, émanant des établissements d'enseignement et de recherche français ou étrangers, des laboratoires publics ou privés.

RTS NOISE DETECTION AND VOLTAGE EFFECT ON RTS IN HgCdTe FOCAL PLANE ARRAY

Maxence Guénin^{1,*}, Sophie Derelle², Marcel Caes², Laurent Rubaldo³, Isabelle Ribet-Mohamed²

¹*Université Paris-Saclay, ONERA, DOTA, F-91123 Palaiseau, France*

²*ONERA/DOA – Chemin de la Vauve aux Granges, 91120 Palaiseau, France*

³*LYNRED, Avenue de la Vauve - CS20018, 91127 Palaiseau Cedex, France*

*maxence.guenin@onera.fr, +33 1 80 38 63 66

Abstract: We developed an automated Random Telegraph Signal detection and characterization method, as well as a blinking noise and slow drift separation method adapted to focal plane arrays. Utilizing these methods, a study of the evolution of the number of RTS pixels and the amplitudes of the blinking signal as a function of the reverse bias voltage and temperature is conducted. It is shown that physical characteristics of RTS follow Arrhenius laws and increase with bias. Finally, the origin of the increase of the amplitude as a function of the reverse bias is discussed.

Keywords: Random Telegraph Signal, 1/f noise, Reverse Bias, Image Quality, Algorithm

INTRODUCTION

Temporal noise is one of the main challenges in the quest for high operability and stability of image quality over time in infrared focal plane arrays (IR FPA). This type of noise cannot be corrected by a classical non-uniformity correction, as parasitic extra-noise signal may vary in time. Among the sources of temporal noise, low-frequency noises, or $1/f^\alpha$ noises, with f being the frequency and α a coefficient between 1 and 2, are part of the main sources of noise restraining the high operating temperature trend in cooled infrared sensors. Random Telegraph Signal (RTS) is one of them. It exhibits significant current variations with seemingly random occurrences in the temporal dimension. It can affect small scale image quality when the jump amplitude exceeds the residual fixed pattern noise and the very longterm stability through its impact on gain/offset correction tables. Therefore, understanding the physics behind this phenomenon is critical to improve cooled sensors' image temporal stability.

Also called “blinking pixel” in the frame of FPAs, RTS pixel exhibits a multi-stable signal, i.e. a signal fluctuating between multiple stable states. Figure 1 shows a bi-stable RTS signal recorded on our FPA. It

27 presents two stable states, separated by a jump characterized by its amplitude A, and with instant lifetimes τ_{up}
 28 and τ_{down} . Mean values of lifetimes $\langle\tau_{up}\rangle$ and $\langle\tau_{down}\rangle$ are commonly used to characterize the blinking frequency.
 29 In the case of a bi-stable RTS, the relation between the blinking lifetimes and the blinking frequency is as
 30 described in Equation (1):

$$f_c = \frac{1}{\langle\tau_{up}\rangle} + \frac{1}{\langle\tau_{down}\rangle} \quad (1)$$

31 RTS has been detected in many types of systems, such as nanowires [1], silicon transistors [2] and
 32 photodectors [3], and IR FPA, such as T2SL [4], InGaAs [5] or HgCdTe [6, 7] detectors. It would be too
 33 simplistic to assume that each RTS behavior in each system is a consequence of the same physical phenomenon.
 34 Thus, this article is solely discussing of the RTS behavior in HgCdTe detectors. Prior results have been
 35 established [6] on this material, proving that the RTS amplitude and lifetimes demonstrated a Boltzmann
 36 behavior, which means it is activated by temperature with an activation energy E_a . The objective of our study is
 37 to further this study with varying bias voltage, in order to highlight a field effect.

38 In the first part of this paper, the algorithm of detection and characterization of the RTS pixels is
 39 presented. It is based on a changepoint detection method, a corner frequency method and a histogram fit method.
 40 The second part is focused on the detection problems raised by the superposition of RTS and other low
 41 frequency noises, and the algorithm developed to tackle this issue. Finally, in the third part of the paper, the
 42 experimental setup and results on activation energy versus bias on a Mid-Wave Infrared (MWIR) detector are
 43 presented.

44 **RTS DETECTION AND CHARACTERIZATION ALGORITHM**

45 The principle of the Algorithm for Advanced RTS Detection (AARD) is presented in figure 2. There are
 46 three paths: the changepoint path, also called the ‘‘Pruned Exact Linear Time’’ (PELT) path, the frequency or
 47 LFNS one, and the histogram fit one. The changepoint path is based on a changepoint detection called PELT
 48 method [8]. It defines a cost function based on the variance of the signal and a threshold for the search in the
 49 mean changes. This threshold Cr is designed as follows:

$$Cr = \max\left(k \cdot MAD(X), \frac{\max(X) - \min(X)}{2k}\right) \quad (2)$$

50 with k being the effective tunable threshold, typically varying between 1 and 3, and MAD being the Median
 51 Absolute Deviation of the signal X. Having a comparison between two criteria, one on the non-Gaussian

52 character of the signal, and one on the maximum amplitude of the noise, makes it possible to detect pixels
 53 showing a high number of jumps with low amplitudes, as well as pixels showing a low number of jumps with
 54 high amplitudes. Then, a State Reduction (SR) algorithm is applied to the extracted signal to compute the final
 55 RTS contribution to the raw temporal signal. As shown in [9], the estimated RTS signal is representative of the
 56 blinking noise, even with multiple stable states and low RTS-to-white-noise ratio. In the following, the
 57 PELT+SR algorithm will be referred simply as PELT.

58 In parallel, the LFNS and the histogram methods are used to verify the RTS nature and behavior of the
 59 pixel. The LFNS method relies on a fit of the power spectral density (PSD) multiplied by the frequency, in order
 60 to flatten the $1/f$ noise and highlight the $1/f^2$ noise. It has been shown that the bi-stable RTS noise had a
 61 Lorentzian frequency signature [10]. In the LFNS plot, the $1/f$ noise is represented by a constant and the $1/f^2$ or
 62 Lorentzian noise shows a peak function which is described by a “Lorentzian times frequency” function as in
 63 Equation (3):

$$f \cdot PSD = \Delta I^2 \langle \tau_{up} \rangle^2 \langle \tau_{down} \rangle^2 \frac{f_c^2 f}{1 + (2\pi f/f_c)^2} \quad (3)$$

64 With ΔI the amplitude of the jump, and f_c the corner frequency of the Lorentzian. This corner frequency is
 65 extracted, and in the case of bi-stable RTS, this corner frequency is the blinking frequency defined in (1). This
 66 study, however, does not focus on frequency characterization, hence this method will only be used in future
 67 studies. Finally, the histogram method is based on the histogram plot of the signal, which shows multiple
 68 Gaussian distributions if the pixels show RTS with white noise. Fitting these distributions and estimating the
 69 difference between consecutive maxima of the fit enable the calculation of the RTS amplitude and the
 70 establishment of a “well defined two-level RTS pixels” list, which are the objects of study in the next part of the
 71 work. These pixels are characterized by well separated Gaussian distributions, which entail jump amplitudes
 72 higher than two times the estimated white noise, and the presence of a minimum between consecutive local
 73 maxima of the histogram.

74 **SENSITIVITY OF THE ALGORITHM TO SLOW DRIFT**

75 By using the three methods presented in the previous section, it is possible to detect random telegraph
 76 pixels, to estimate and verify their jump amplitude, lifetimes and frequencies, and to extract a list of well-defined
 77 two-level pixels. However, despite having low error in the case of pure RTS + white noise, one of the drawbacks
 78 of this technique is that it may be sensitive to slow drift, which has a frequency behavior of $1/f^\alpha$, with $1 < \alpha < 2$. In

79 practice, this drift can be the cause of false detections or high error RTS estimations. An illustration of the effect
80 of the drift on the signal, on the RTS signal estimated with PELT and on its associated histogram is given in
81 Figure 3. We can clearly see an increase of the error in the estimated level number of the RTS signal.

82 In order to quantify this error, we used a Monte Carlo method to generate different 2 levels RTS signals.
83 Input parameters are mean lifetimes $\langle\tau_{up}\rangle$ and $\langle\tau_{down}\rangle$ (described by an exponential distribution as reported in
84 [11]), jump amplitude A_{RTS} , drift amplitude A_{DRIFT} (we assumed a linear behavior for the present study) and a
85 white temporal noise. After applying PELT method to these signals, we classify our results as follows: a non-
86 detection (ND) is a failure of the algorithm to detect a pixel which is RTS. A false detection (FD) is a detection
87 of a pixel which is not RTS but is detected as such by the algorithm. Finally, a correct detection (CD) is a
88 detection of an RTS pixel as such, and a correct non detection (CND), a detection of a non RTS pixel as such. In
89 this study, fixed input parameters are: the length of the sample, which is 10^4 frames, the white noise considered
90 equal to 10 digits rms (similar to the detector studied in a subsequent section) and the mean lifetimes which are
91 100 frames. We simulated 10 jump amplitudes ranging from 0 to 200 digits and 6 drift peak-to-peak amplitudes
92 ranging from 0 to 100 digits. For each (A_{RTS}, A_{DRIFT}) condition, we generated 10 distinct RTS signals leading to
93 a total of 600 simulated pixels. First, a preliminary study has been conducted, where the k factor in the Cr
94 criterion is ranging from 0.5 to 3. For pixels without drift, a low k leads to 0% ND and 0% FD and in these
95 cases, PELT is a very robust method. However, when increasing drift, low k brings higher ND and FD
96 percentages than high k, hence this factor needs to be optimized.

97 We obtained a qualitative color map of the average output of the PELT algorithm as a function of the
98 jump amplitude and drift amplitude, as shown in figure 4a). The color and hashes of each cell correspond to the
99 more probable state (ND, FD, CD or CND) of the 10 distinct RTS signals obtained with the same (A_{RTS}, A_{DRIFT})
100 condition. On the 600 simulated pixels, we finally obtain 50% FD and 8.9% ND. However, some correct RTS
101 detections are due to the drift and not to the detection of a transition between up and down levels. The
102 corresponding pixels are shown in green cells marked by crosses. They represent 22% of the distribution and
103 present an A_{RTS}/A_{DRIFT} ratio lower than 1. This is consistent with results obtained with the Gaussian method,
104 where 75% of the simulated pixels are detected as “well defined two-level RTS”. In addition, 23% of the RTS
105 pixels (marked by circles) show strong errors between the estimated RTS signal and the raw data. In these cases,
106 high drift systematically increases the estimation errors on the number of levels and/or the jump amplitudes
107 and/or the lifetimes, thus increasing the characterization output error.

108 In order to reduce the PELT method output error, the Drift And RTS Characterization, Separation by
109 Overall, Unique Level Selection (DARCSOULS) algorithm has been developed to discriminate the blinking
110 signal from the slow drift. The principle of the algorithm is presented in figure 5. It is based on the hypothesis
111 that the amplitude of the drift is negligible over the course of a few RTS jumps. PELT is applied locally on small
112 pieces of the signal. Then the overall number of levels is estimated with the median value of the local number of
113 levels, which allows the compensation of the RTS signal. The drift is calculated by applying a low-pass filter to
114 the remaining signal. Finally, the extracted RTS signal is obtained by subtracting the calculated drift from the
115 raw signal and applying PELT on the overall extracted signal.

116 An optimization between the computation time, the number of slices according to the mean lifetimes
117 has been conducted. Continuing the previous study, a color map of the average output of the
118 PELT+DARCSOULS algorithms is shown in figure 4b. We consider the group $\{P_0\}$ of N_0 pixels that were
119 incorrectly characterized after applying the PELT method and the group $\{P_1\}$ of N_1 pixels from $\{P_0\}$ which are
120 correctly characterized after applying DARCSOULS algorithm. The recovery rate is: $RR=N_1/N_0$. In this study, it
121 is equal to 62%. The remaining 38% are: pixels with too low jump amplitude-to-white noise ratio, thus creating
122 non detections (19%), or pixels with too low jump amplitude-to-drift amplitude ratio, thus preventing the correct
123 separation of drift and RTS and increasing the characterization output error (19%). For the Gaussian method, the
124 detection rate of “well behaved two level RTS pixels” after applying DARCSOULS is increased to 81% (6%
125 increase).

126 In most of cases, applying AARD and DARCSOULS is enough to extract low error RTS amplitudes
127 lifetimes and frequencies. In conclusion, these algorithms have enabled an automatic detection and
128 characterization of the blinking pixels for the experimental study of the influence of the bias voltage on RTS
129 signals.

130 **INFLUENCE OF THE BIAS VOLTAGE ON THE RTS PIXELS NUMBER AND** 131 **ACTIVATION ENERGY OF THE AMPLITUDE**

132 The experimental FPA consists in a MWIR 15 μ m pitch n-on-p HgCdTe detector. Its cut-off wavelength
133 at 80K is $\lambda_c=5.3\mu$ m. The detector is placed inside a continuous flow nitrogen cryostat, with an integrated heating
134 system, enabling the control of the temperature with a precision of 30mK peak-to-peak. The detector is placed in
135 front of an extended blackbody at $T_{BB}=298$ K with an optical aperture of f/8. Data cubes of 8000 images are

136 acquired with an integration time of 15ms, which also represents the interval between two images, as the detector
 137 is used in Integrate While Reading mode. The detector temperature varies between 110K and 122K, with a 3K
 138 step, and the bias voltage varies between V_0 and $V_0+0.3V$, with a 0.06V step and V_0 being the nominal reverse
 139 bias value. For this study, both types of protocol were explored: fixed reverse bias with varying temperature, and
 140 fixed temperature with varying reverse bias. As a summary, each experiment consists of 30 measurements, with
 141 a total observation time of 72 minutes, corresponding to $2.9 \cdot 10^5$ images to process.

142 First, the data cubes are processed through the AARD algorithm that allows the estimation of the
 143 number of RTS pixels of the FPA. In figure 6, the evolution of the number of RTS pixels in the detector as a
 144 function of the temperature and bias voltage is presented. In figure 6a), it is shown as a function of the bias
 145 voltage with different temperatures, and in figure 6b), it is shown as a function of the temperature with different
 146 bias voltage. In the former, it is clear that the increase in bias voltage increases the number of RTS pixels, but a
 147 fitting physical model has yet to be determined. It is yet clear that the rate of increase in function of the bias
 148 decreases with increasing temperature. A saturation effect may be considered. In figure 6b), it is possible to fit
 149 the different curves with an Arrhenius law, defined as follows:

$$X = X_0 e^{-\frac{E_a}{k_B T}} \quad (4)$$

150 With X a physical quantity ($X=N$ in the case of the number of RTS and $X=A$ in the case of the
 151 amplitude), X_0 a factor homogenous to X (which can depend on V_{bias}), E_a an activation energy, k_B the
 152 Boltzmann constant, and T the temperature of the detector. The fit shows that the number of RTS follows a
 153 Boltzmann law whichever the bias voltage is. The extracted activation energy is decreasing with increasing bias
 154 voltage; however, this is not directly interpretable, as the number of RTS detected is strongly dependent on
 155 different parameters, such as detection thresholds and RTS state definitions.

156 In a second study, the acquired data cubes are processed through the AARD and DARCSOULS
 157 algorithm in order to extract the evolution of the amplitude with the temperature and the bias voltage. Pixels that
 158 show too low amplitude to white noise ratio, display incorrigible drift or are simply false detections are manually
 159 removed, as the amplitudes cannot be estimated correctly in these cases. As an example, for two pixels, the
 160 amplitude as a function of the inverse of temperature is presented in figure 7 for different bias voltage. It shows
 161 that the amplitude increases with the bias voltage. In addition, whatever the voltage, the RTS amplitude follows
 162 an Arrhenius law, from which an activation energy can be extracted. These results are coherent with previous
 163 works [6].

164 The plot of the evolution of the Arrhenius activation energy as a function of bias voltage, for all the
165 RTS pixels detected and studied is shown in figure 8. As shown on the graph, each pixel behaves differently and
166 it would not be appropriate to study the RTS amplitude on the whole group of pixels. Two behaviors have been
167 observed: pixels with decreasing activation energy as a function of bias, and pixels with constant activation
168 energy as a function of bias. While keeping in mind that the amplitude increases with bias voltage for most of the
169 pixels studied and the Arrhenius law defined in Equation (4), we can deduce that the pre-exponential factor of
170 amplitude A_0 is also a contributor of the evolution of the amplitude. A_0 is a function of the reverse bias. The
171 evolution of the amplitude as a function of bias is a non-trivial combination of the evolution of the factor A_0 and
172 the evolution of the activation energy E_a contributions. We can hypothesize that high variations of the activation
173 energy are due to the thermodynamic barrier associated with the jump being reduced along the increase in
174 applied bias. It has already been shown that RTS was related to defects in the material [12]. A Poole-Frenkel
175 [13] model could be considered, in which a dissymmetry of the band diagram around the defect implied in the
176 process appears while applying a voltage to the system, thus lowering the barrier. In the case of low variation of
177 activation energy, the results could go in favor of the Kinch model [14], with an enhancement of tunneling by the
178 increase of the reverse bias. Also, according to this model, this could be due to the extension of the depletion
179 region, caused by the reverse bias increase, in other words an extension of the cross-section that the diode
180 depletion region presents to defects at the origin of RTS.

181

182 **CONCLUSION**

183 An RTS detection and characterization algorithm as well as a RTS and slow drift separation algorithm
184 have been presented. They have then been used to characterize the evolution of the number of blinking pixels
185 and blinking amplitudes as a function of temperature and bias voltage. It has been confirmed that the blinking
186 process is characterized by an activation energy whichever bias voltage is applied, for the number of RTS pixels
187 and the amplitudes of blinking. The RTS number and the amplitude increase with the bias voltage. The
188 amplitude activation energy either decreases or stays constant with increasing reverse bias voltage. Physical
189 models for either the evolution of the number of RTS with bias or the evolution of the amplitude with bias have
190 yet to be developed. This study will be extended the blinking lifetimes and frequencies with PELT and LFNS
191 methods in order to obtain a better understanding of the physics behind the RTS phenomenon in HgCdTe and
192 bias effects.

193 **FUNDINGS**

194 This work has been partially supported by ED572 doctoral school of Paris-Saclay University.

195 **CONFLICT OF INTEREST**

196 The authors declare that they have no conflict of interest.

197 **REFERENCES**

198 [1] Y. Kutovyi, I. Zadorozhnyi, N. Naumova, N. Boichuk, and M. Petrychuk in 25th International Conference on
199 Noise and Fluctuations (ICNF 2019) (2019).

200 [2] S.T. Hsu, Solid State Electron. 14, 487(1971).

201 [3] V. Goiffon, G.R. Hopjinson, P. Magnan, F. Bernard, G. Rolland, O. Saint-Pé, IEEE T. Nucl. Sci. 56, 4
202 (2009).

203 [4] I. Ribet-Mohamed, J. Nghiem, M. Caes, M. Guénin, L. Höglund, E. Costard, J.B. Rodriguez and P. Christol,
204 Infrared. Phys. Techn., 96, 145 (2019).

205 [5] D. Pogany, G. Guillot, Microelectron Reliab. 39, 341 (1999).

206 [6] A. Brunner, L. Rubaldo, V. Destefanis, F. Chabuel, A. Kerlain, D. Bauza and N. Baier, J. Electron. Mater.
207 43, 8 (2014).

208 [7] R. Kohley, R. Barbier, J.-C. Clémens, L. Conversi, P.-E. Crouzet, A. Ealet, S. Ferriol, W. Gillard, B. Kubik,
209 C. Rosset, A. Secroun, B. Serra, P. Strada, Proc. SPIE 10709, High Energy, Optical, and Infrared Detectors for
210 Astronomy VIII, 107091G (2018)

211 [8] R. Killick, P. Fearnhead and I.A. Eckley, J. Am. Stat. Assoc. 107,500,1590-1598 (2012).

212 [9] M. Guénin, S. Derelle, M. Caes, L. Rubaldo and I. Ribet-Mohamed in 25th International Conference on
213 Noise and Fluctuations (ICNF 2019) (2019).

214 [10] B.K. Jones, IEEE Trans. Electron. 41, 11 (1994).

215 [11] Y. Yuzhelevski, M. Yuzhelevski and G. Jung, Rev. Sci. Instrum, 71, 1681 (2000).

216 [12] P. Guinedor, A. Brunner, L. Rubaldo, D. Bauza, G. Reibold and D. Billon-Lanfrey, J. Electron. Mater. 48,
217 6113 (2019).

218 [13] J. Frenkel, Phys. Rev. 54, 647 (1938).

219 [14] M.A. Kinch, C.-F. Wan, H. Schaake, and D. Chandra, Appl. Phys. Lett. 94, 193508 (2009)

220 **FIGURES CAPTIONS**

221 Figure 1: Typical behavior of a bi-stable RTS pixel. The straight line represents the signal. Dashed lines
222 represent the levels mean value.

223 Figure 2: Schematic principle of the Algorithm for Advanced RTS Detection, with the PELT algorithm, State
224 Reduction(SR) algorithm, LFNS method and Gaussian method.

225 Figure 3: Effect of the drift on the signal (left) and on the associated histograms (right)

226 Figure 4: Qualitative color map of the output of a) the PELT algorithm, b) the PELT+DARCSOULS algorithms.
227 A green cell corresponds to a major CD output; a red, vertically hashed one to a ND output; a blue, diagonally
228 hashed one to a CND output and an orange, horizontally hashed one to a FD output. Crossed cells represent
229 pixels detected due to the drift. Circles represent a strong error in the estimation of the RTS parameters.

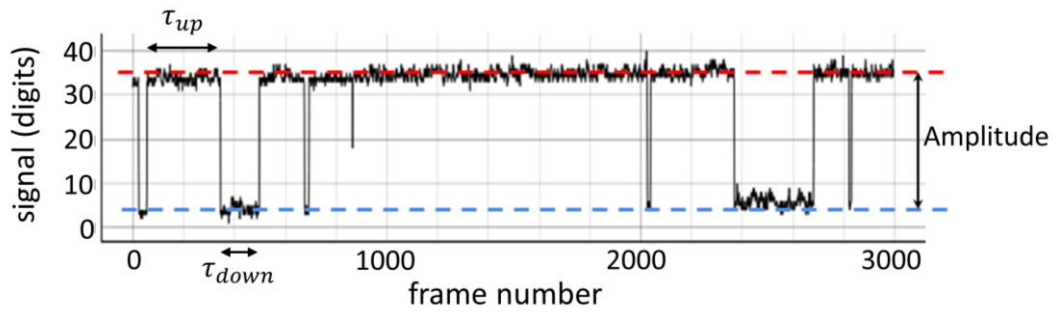
230 Figure 5: a) Schematic principle of the RTS – drift separation algorithm b) Upper blue curve: RTS + drift
231 simulated signal. In red: local PELT estimation. Lower blue curve: signal with RTS compensation, equivalent to
232 slow drift with white noise. Green straight line: low pass filter of the lower blue curve, which is the estimated
233 slow drift. c) RTS signal extracted from b) by subtracting the low frequency signal from the original signal. In
234 orange binary signal is the final PELT estimation of the RTS in the pixel.

235 Figure 6: a) Normalized number of RTS pixels in the FPA as a function of bias voltage for different
236 temperatures. ΔV is the interval between the true bias and a reference bias V_0 , such as $V_{\text{bias}} = V_0 + \Delta V$. b)
237 Normalized number of RTS pixels in the FPA as a function of temperature for different bias voltages. Dashed
238 lines are respective Arrhenius fits for each bias.

239 Figure 7: RTS amplitude as a function of $1/T$ and the Arrhenius plots for several bias voltages of two different
240 pixels of the FPA.

241 Figure 8 Evolution of the activation energy for amplitude as a function of the reverse bias voltage for all the
 242 studied RTS pixels for low variation pixels (a) and high variation pixels (b)). Each curve is a different pixel.

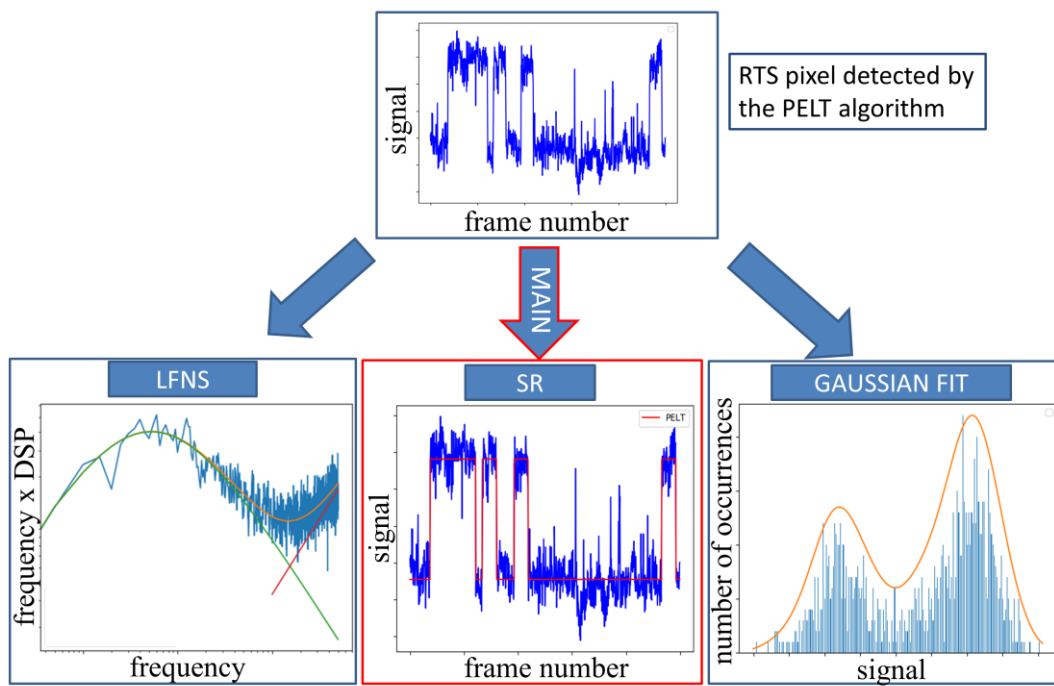
243 **FIGURES**



244
 245

246

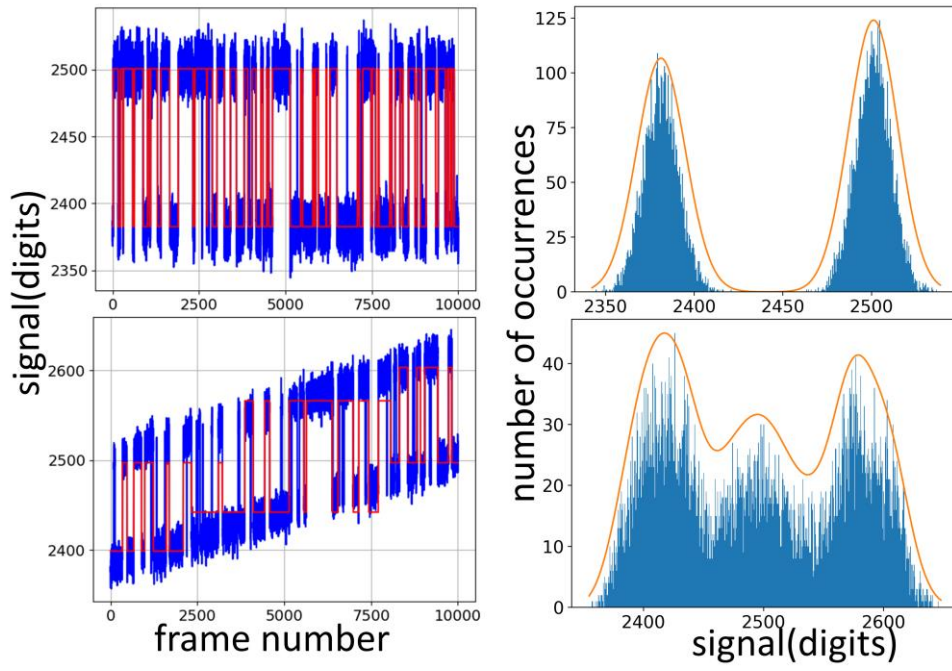
Figure 1: Guénin et al.



247

248

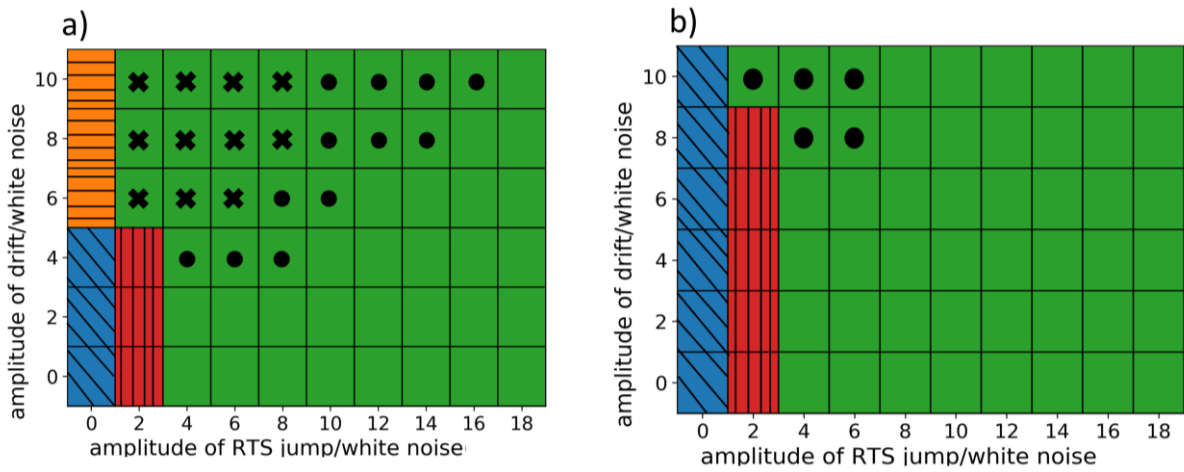
Figure 2: Guénin et al.



249

250

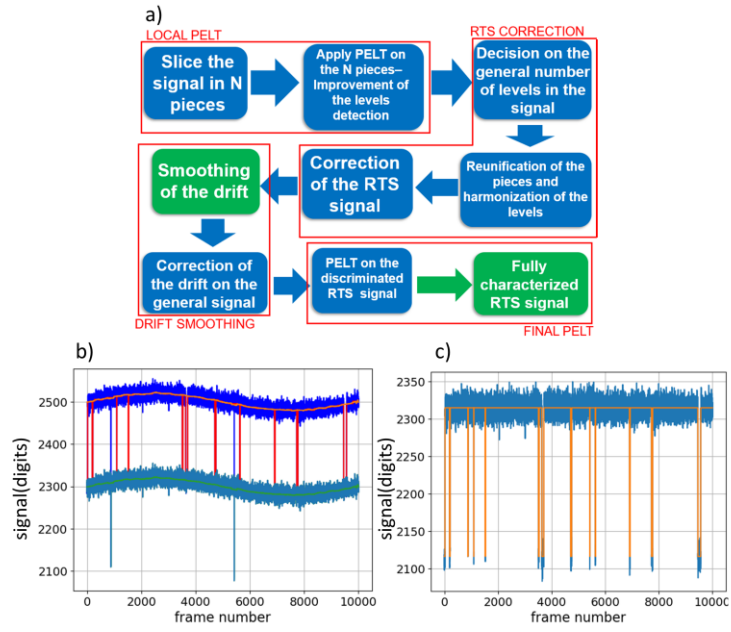
Figure 3: Guénin et al.



251

252

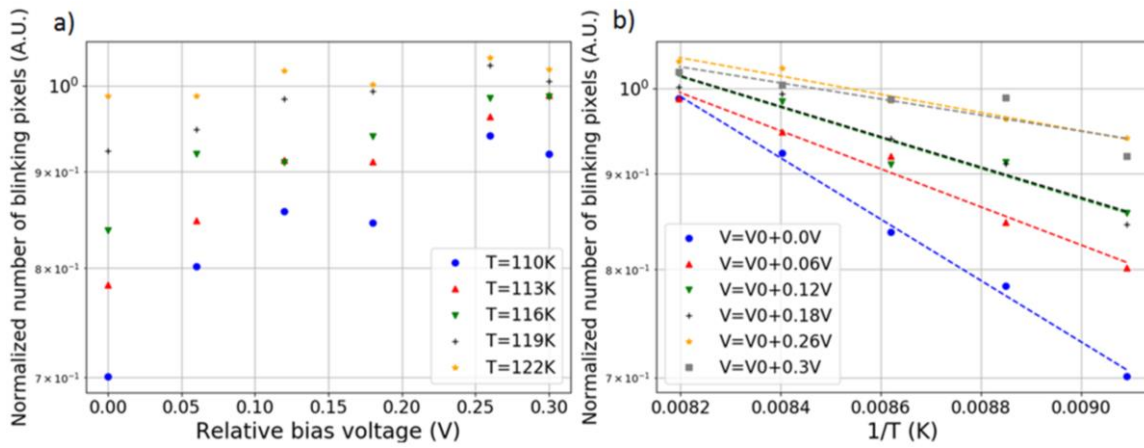
Figure 4: Guénin et al.



253

254

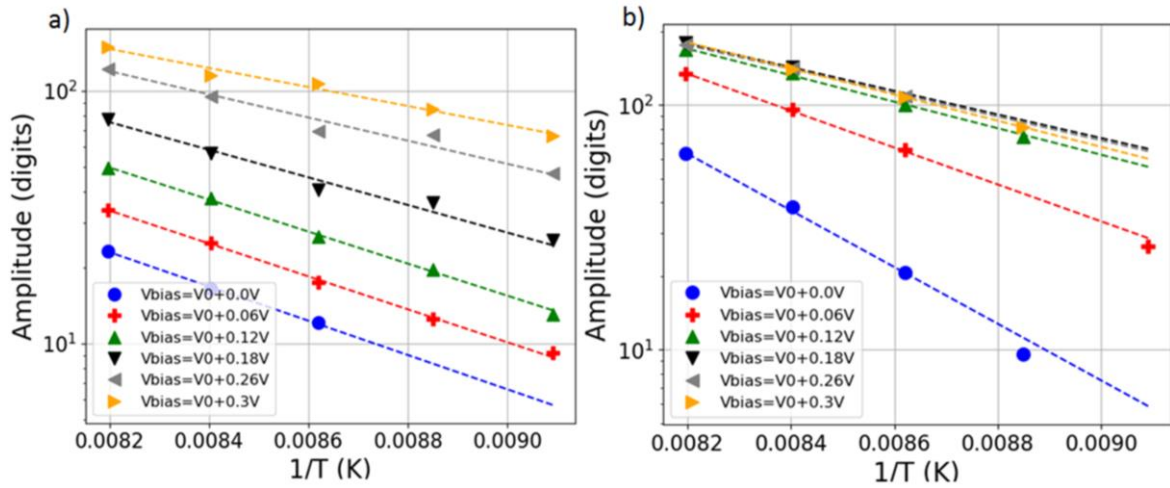
Figure 5: Guénin et al.



255

256

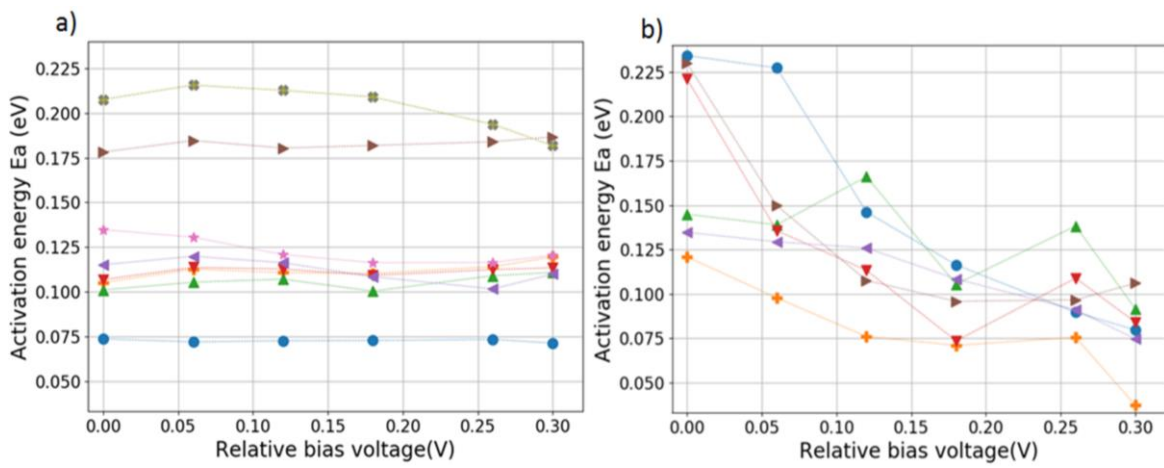
Figure 6: Guénin et al.



257

258

Figure 7: Guénin et al.



259

260

Figure 8: Guénin et al.